Journal of Solid State Chemistry 184 (2011) 2902–2908

Contents lists available at SciVerse ScienceDirect

Journal of Solid State Chemistry

journal homepage: www.elsevier.com/locate/jssc

Synthetic approaches to borocarbonitrides, BC_xN ($x=1$–2)

Nitesh Kumar, Kalyan Raidongia, Abhishek K. Mishra, Umesh V. Waghmare, A. Sundaresan, C.N.R. Rao *

Chemistry and Physics of Materials Unit, CSIR Centre of Excellence in Chemistry and International Centre for Materials Science, Theoretical Sciences Unit, Jawaharlal Nehru Centre for Advanced Scientific Research, Jakkur, Bangalore 560064, India

ARTICLE INFO

Article history:
Received 25 July 2011
Received in revised form
24 August 2011
Accepted 25 August 2011
Available online 10 September 2011

Keywords:
Borocarbonitrides
Vapor phase synthesis
Nanopans
First principles calculations

ABSTRACT

In order to synthesize borocarbonitrides of the general formula BC_xN where x varies between 1 and 2, we have carried out high-temperature gas phase reaction of BBr_3 with a mixture of ethylene and ammonia. The composition of the product was close to $BC_{1.6}N$ as shown by x-ray photon spectroscopy (XPS) and electron energy loss spectroscopy (EELS). The products were further characterized by infrared, Raman and other spectroscopic techniques. The borocarbonitrides obtained from the gas phase reaction have low surface areas, in contrast to those of similar compositions prepared by the urea method. First principles calculations show that the most stable structures of the compositions BCN and BC_2N contain BN-rich and carbon-rich domains where BN_3 and NB_3 units are present.

1. Introduction

Emergence of graphene as an exciting two-dimensional material has propelled research on analogous layered inorganic materials. Thus, recently graphene-like MoS_2 and BN have been synthesized and characterized [1,2]. Hexagonal borocarbonitrides of the general formula $B_xC_yN_z$ have attracted interest recently. $B_xC_yN_z$ is expected to possess properties intermediate between graphene and BN, which can be tuned by varying the carbon content as well as by changing the structural characteristics [3–6]. There are a few reports on the synthesis of $B_xC_yN_z$ type materials in the form of nanotubes by chemical vapor deposition (CVD), using transition metal nanoparticles as catalysts and also by methods such as arc-discharge and laser ablation [7–13]. Jansen and co-workers [14,15] have synthesized Si–B–N–C ceramics using molecular precursors. There is, however, limited information available on the borocarbonitrides, $B_xC_yN_z$, with well-defined compositions. Vinu et al. [16] reported mesoporous BCN obtained by the reaction of B_2O_3 and mesoporous carbon at very high temperatures under flowing nitrogen. Raidongia et al. [17] prepared a borocarbonitride of the composition $BC_{1.5}N_{1.1}$ by heating urea, boric acid and high-surface area activated charcoal in an inert atmosphere. Ci et al. [18] have synthesized layers of $B_xC_yN_z$ with separated graphene and BN domains by the reaction between NH_3–BH_3 complex and methane. In view of the marginal success in synthesizing $B_xC_yN_z$ materials and the potential uses of these materials, we have carried out vapor phase synthesis of $B_xC_yN_z$ by taking BBr_3, ethylene and ammonia as the sources of boron, carbon and nitrogen, respectively. Our interest has been to synthesize borocarbonitrides with compositions in the vicinity of BCN or BC_2N. A vapor phase synthesis of BCN was carried out by Kaner et al. [19] some years ago by the reaction of acetylene, BCl_3 and NH_3. These authors could not characterize the product adequately. We have prepared BC_xN ($x=1$–2) compositions by the gas phase reaction of ethylene, BBr_3 and NH_3 and compared their characteristics with those of similar compositions obtained by the reaction of activated carbon, boric acid and urea. We have also carried out first-principles calculations on the stable structures of BCN and BC_2N.

2. Experimental

2.1. Gas phase synthesis of BC_xN

Gas phase synthesis of composition BC_xN was carried out using liquid BBr_3, high purity ammonia gas and 20% ethylene gas mixed with nitrogen as the sources of boron, nitrogen and carbon, respectively. The experimental set up for the reaction is shown in Fig. 1. In this set-up, nitrogen gas, which acts as the carrier gas bubbles through liquid BBr_3 and carries its vapor into the hot zone of the tube furnace. In the hot zone, BBr_3 reacts with the mixture of ammonia and ethylene gas coming from the other two inlets. A quartz boat present in the hot zone was used to collect the deposited product. At the end of the boat, we keep a circular glass slide in order to keep the gaseous reactants in the hot zone. Before starting the reaction, the quartz tube was purged with ammonia for 30 min. The furnace temperature was set to 950 °C at the rate of

* Corresponding author. Fax: +91 80 22082760.
E-mail address: cnrrao@jncasr.ac.in (C.N.R. Rao).

0022-4596/$ - see front matter © 2011 Elsevier Inc. All rights reserved.
doi:10.1016/j.jssc.2011.08.034

7 °C/min. When the temperature reached to 850 °C, nitrogen gas was allowed to bubble through the liquid BBr_3 and the flow of ethylene also started at this temperature. The furnace was maintained at 950 °C for 1 h with the reactants. The supply of BBr_3 and ethylene was stopped, but the ammonia gas flow was continued till the furnace attained room temperature. The product deposited in the quartz boat was heated at 750 °C in an inert atmosphere for 5 h in order to remove traces of NH_4Br in the product.

2.2. Synthesis of BC_xN by the urea route

In the urea route, 0.1 g boric acid and 0.5 g high surface area activated charcoal (1250 m^2/g) were mixed with varied amount of urea in order to keep the molar ratio of boric acid to urea from 1:6 to 1:24. The mixture was heated at 900 °C for 12 h in an inert atmosphere. The product obtained was heated again at 930 °C in an ammonia atmosphere for 3 h.

2.3. Characterization

X-ray diffraction of the samples were carried out by Bruker-D8 X-ray diffractometer using Cu $K\alpha$ radiation. FESEM images were obtained using FEI Nova-Nano SEM-600, The Netherlands. TEM and HRTEM analyses were carried out by FEI TITAN3 80–300 kV aberration corrected transmission electron microscope. Quantification of the electron energy loss spectra (EELS) was possible with a Gun monochromator (resolution better than 0.3 eV), camera length 73 mm and GIF aperture 1 mm, which gives collection angle ~3.336 mrad. AFM measurements were performed using NanoMan instrument in the tapping mode. XPS was performed in ESCALAB MKIV spectrometer employing Al $K\alpha$ (1486.6 eV) as photon source. IR spectra were recorded by a Bruker IFS 66 v/S spectrometer. Raman spectroscopy was carried out in a LabRAM HR with a 633 nm line from a HeNe laser. TGA was performed in Mettler Toledo Star system. Nitrogen adsorption–desorption measurements were carried out in a QUANTACHROME AUTOSORB-1C instrument.

2.4. First-principles calculations

We have used plane-wave self consistent field (PWSCF) [20] implementation of density functional theory (DFT) with a generalized gradient approximation (GGA) [21] to exchange correlation energy of electrons and first-principles ultra-soft pseudopotentials [22] to represent interaction between ionic cores and valence electrons. Kohn–Sham wave functions were represented with a plane wave basis with an energy cut off of 35 Ry and charge density cut off of 210 Ry. Integrations over Brillouin zone were sampled with $16\times4\times1$, $8\times8\times1$ and $4\times8\times1$ meshes of k points in different unit cells chosen depending on their size, shape and occupation numbers were smeared using Methfessel–Paxton scheme [23] with broadening of 0.006 Ry. To simulate various configurations of chemical ordering of B and N, we consider supercells consisting of 8 and 16 atoms with 10 symmetry inequivalent configurations of BC_2N, and use six different configurations with 18 atoms supercell of BCN [17] for comparison (see Fig. 2(a) and (b), respectively). We determined the structure for each configuration through optimizing the energy with respect to atomic positions as well as the size and shape of the supercell.

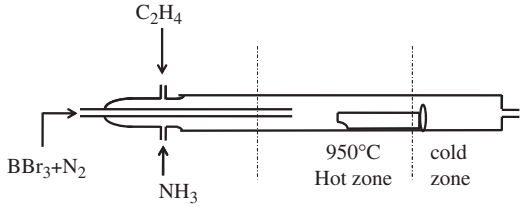

Fig. 1. Schematic of the experimental set-up for gas phase synthesis of BCN.

3. Results and discussion

For the gas phase synthesis of BC_xN, we have employed the reaction of BBr_3 with a mixture of CH_4 and NH_3 at high temperatures. The product of the reaction was analyzed by x-ray photoelectron spectroscopy (XPS) to determine the elemental composition. We show typical core-level spectra of one of the samples in Fig. 3(a), with B (1s), C (1s) and N (1s) with peaks centered at 191.5, 284 and 399 eV respectively. The B (1s) signal can be deconvoluted into two peaks at 190.5 and 192 eV corresponding to boron atoms bonded to carbon and nitrogen, respectively. The C (1s) signal can be deconvoluted to three peaks centered at ~284, 286 and 290 eV corresponding to carbon atoms bonded to boron, carbon and nitrogen, respectively. The N 1s signal can be deconvoluted into two peaks at 397.5 and 400 eV corresponding to nitrogen atoms bonded to boron and carbon, respectively. From the areas under the 1s features, we obtained the elemental composition B:C:N to be 1:1.6:1 after taking the relevant capture cross sections into account. We also obtained a composition BC_xN with $x=1.8$ by the vapor phase method at 950 °C under a flow of 200 sccm (standard cubic centimeter) of ammonia, 40 sccm of 20% C_2H_4 in N_2 and 40 sccm of N_2 through BBr_3. Core level XP spectra of B, C and N of this composition are shown in Fig. 3(b). Our XPS data are well supported by the first-principles calculations.

In order to ensure the compositions of the $B_xC_yN_z$ products obtained by the gas phase reaction, electron energy loss spectroscopy (EELS) was carried out in several regions of the sample. In Fig. 4, we show the spectrum of one of the samples showing K shell ionization edges. The EELS peaks are split into two peaks corresponding to the π^* and σ^* bands showing thereby that boron, carbon and nitrogen atoms are all in the sp^2 hybridized

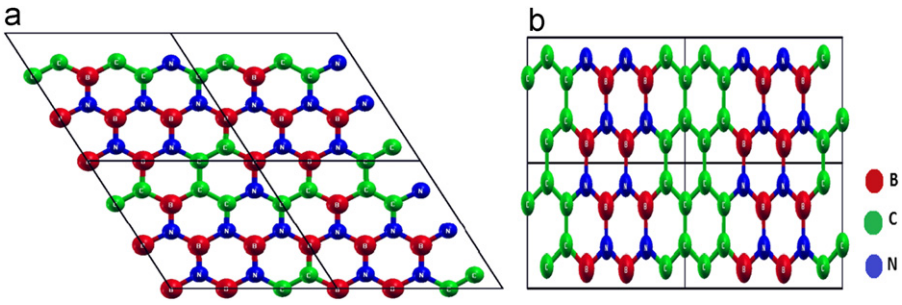

Fig. 2. Most stable structures of BCN (a) and BC_2N (b).

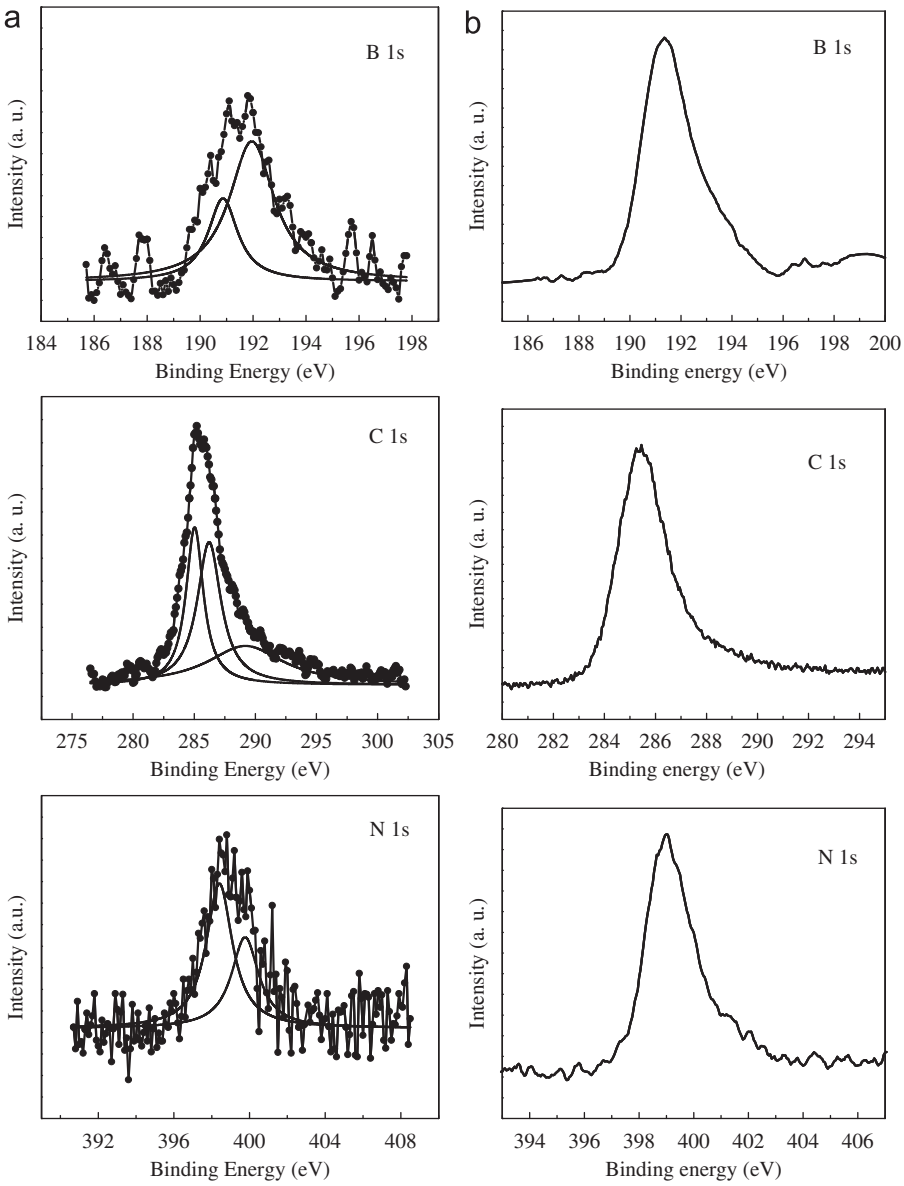

Fig. 3. (a) XPS of gas phase synthesized BCN and (b) XPS of gas phase synthesized BCN under controlled flow rates of gases.

state. Based on the EELS data, the composition was estimated to be B:C:N as 1:2:1. Some regions of the samples gave compositions close to 1:1:1. A spectrum corresponding to this composition is shown in the inset of Fig. 4. The composition obtained by XPS corresponding more to an average composition is between the above two compositions obtained by EELS. If we take the composition of the product to be BC_2N, we can write the reaction for the formation as,

$$BBr_3(g)+C_2H_4(g)+NH_3(g)\rightarrow BC_2N(s)+3HBr(g)+2H_2(g)$$

If we take the composition as BCN, the reaction will be,

$$BBr_3(g)+1/2C_2H_4(g)+NH_3(g)\rightarrow BCN(s)+3HBr(g)+H_2(g)$$

For purpose of convenience we shall describe the product as BCN in the remaining of the text.

We predict the most stable structures of BC_2N and BCN based on our calculations. Lattice constants of the different configurations considered for the composition BC_2N are within 1% of each other, and it is evident that the presence of interlinked local structural motifs of BN_3 and NB_3 is a characteristic feature of the lowest energy configurations [17]. This is understandable in terms of ionic charges of B and N, and the stability of end-members (BN and graphene). Such local structural features are responsible for the stability of domains of BN-rich region interfacing with graphene matrix (see Fig. 2(a) and (b)). Among all the configurations considered, we find that the configuration involving an arm-chair type of an interface between BN-rich and carbon-rich regions are energetically favorable. We note that such a configuration involves inter-connected BN_3 and NB_3 local structures, similar to those discussed earlier [24,25], and a nonpolar boundary between the BN-rich and the carbon-rich domains (Fig. 2 (b)). Similar interlinking of such moieties has been noted by Yamamoto et al. [26] in thick borocarbonitride coatings. It is to be noted that there are only C–C, C–N, B–N and B–C bonds in these structures, but no B–B and N–N bonds.

Substitution of B and N for the 66.7% of carbon atoms (two thirds of carbon atoms) in BCN and 50% (half of the carbon atoms) in BC_2N results in an expansion of the graphene lattice by about 1.5–2%. The cohesive energy of the lowest-energy configuration of BC_2N is 8.77 eV/atom, which is intermediate to the cohesive energies of lowest-configuration of BCN (8.61 eV/atom) and

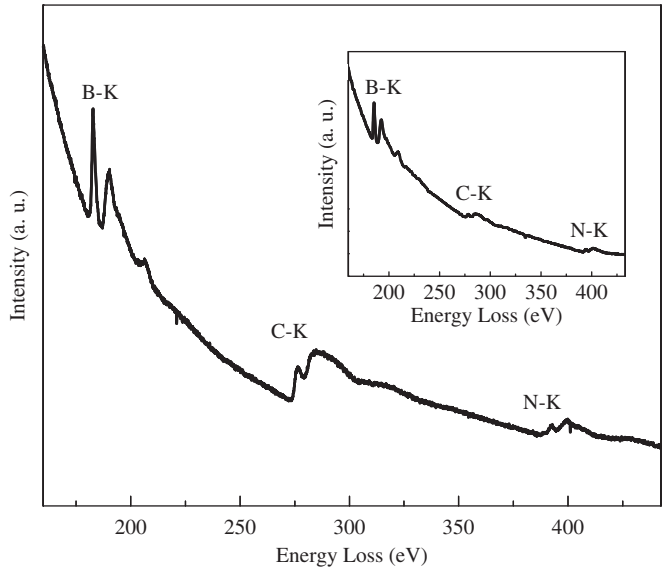

Fig. 4. EELS of a sample of composition $BC_{1.6}N$. The inset shows the corresponding spectrum of composition BCN.

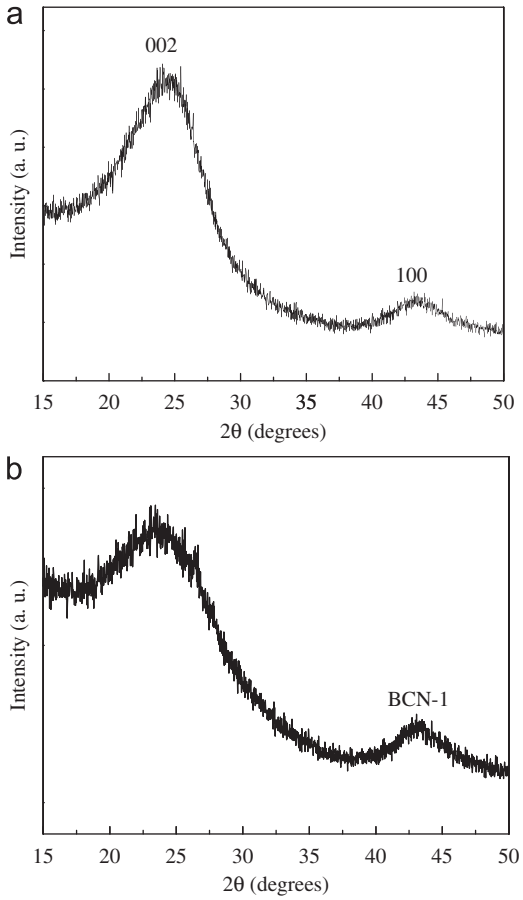

Fig. 5. (a) XRD pattern of BC_2N sample prepared by gas phase reaction and (b) XRD pattern of the sample prepared by urea method.

BC_4N (8.93 eV/atom) [24,25], however noticeably smaller than the cohesive energy of graphene (9.16 eV/atom), estimated within the same computational framework.

BCN obtained from the gas phase reaction gives a broad x-ray diffraction (XRD) pattern as shown in Fig. 5(a). The (002) and (100) reflections, respectively, correspond to the interlayer separation and the in-plane parameter of hexagonal structure. The (002) peak is at a slightly lower 2θ value than bulk BN indicating a larger interlayer separation. From the broadening of the (100) peak, we estimate the average particle size to be $\sim$30 nm.

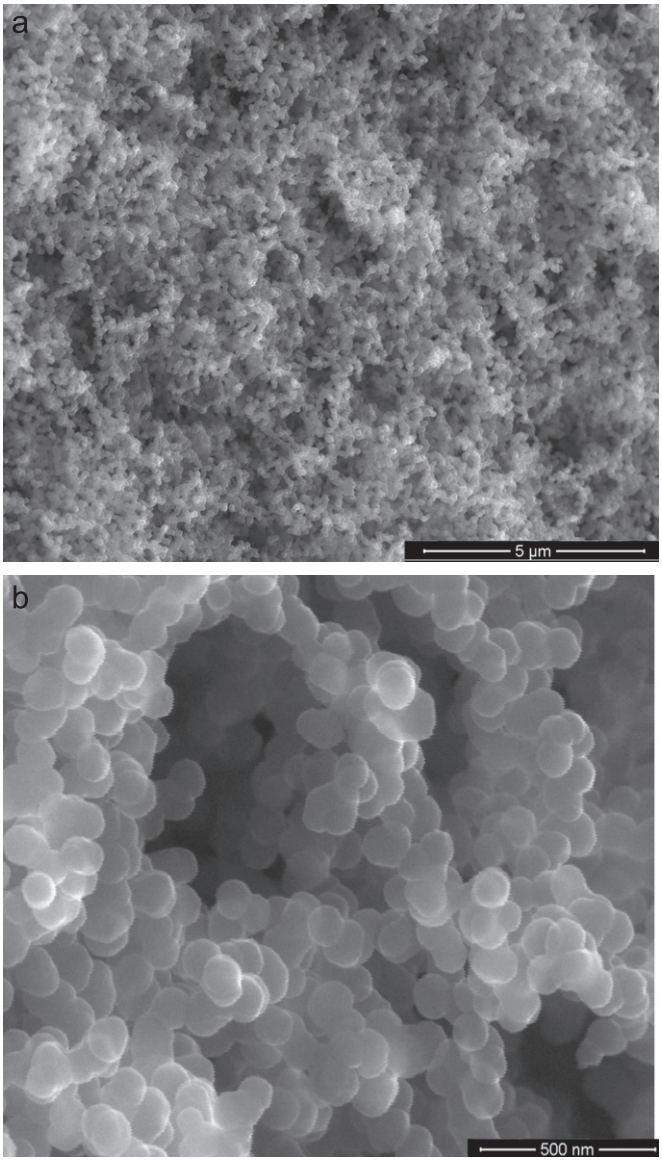

Fig. 6. FESEM images of the samples prepared by gas phase reaction.

In Fig. 6, we show field emission scanning electron microscope (FESEM) images of BCN showing spherical shaped particles with an average diameter of 100 nm. A transmission electron microscope (TEM) image of BCN is shown in Fig. 7(a). We see that the real shape of the BCN particles corresponds to that of nanopans with inner and outer diameters of approximately 50 and 100 nm, respectively. The high-resolution TEM (HRTEM) image in Fig. 7(b) at the rim of the particle shows presence of layers. The interlayer separation is $\sim$3.4 Å, which is slightly larger than that in hexagonal BN. In Fig. 8, we show an atomic force microscope (AFM) image of one of the nanopans along with the height profile. It shows a dip at the center as expected of a pan, the thickness of this center region corresponding to a monolayer. The rim portion shows a height of $\sim$7 Å corresponding to two layers of BCN. We do not fully understand the mechanism of the formation of round shape nanoparticles in our synthesis. However, curling of the basal planes is observed in the past in graphite-like structures

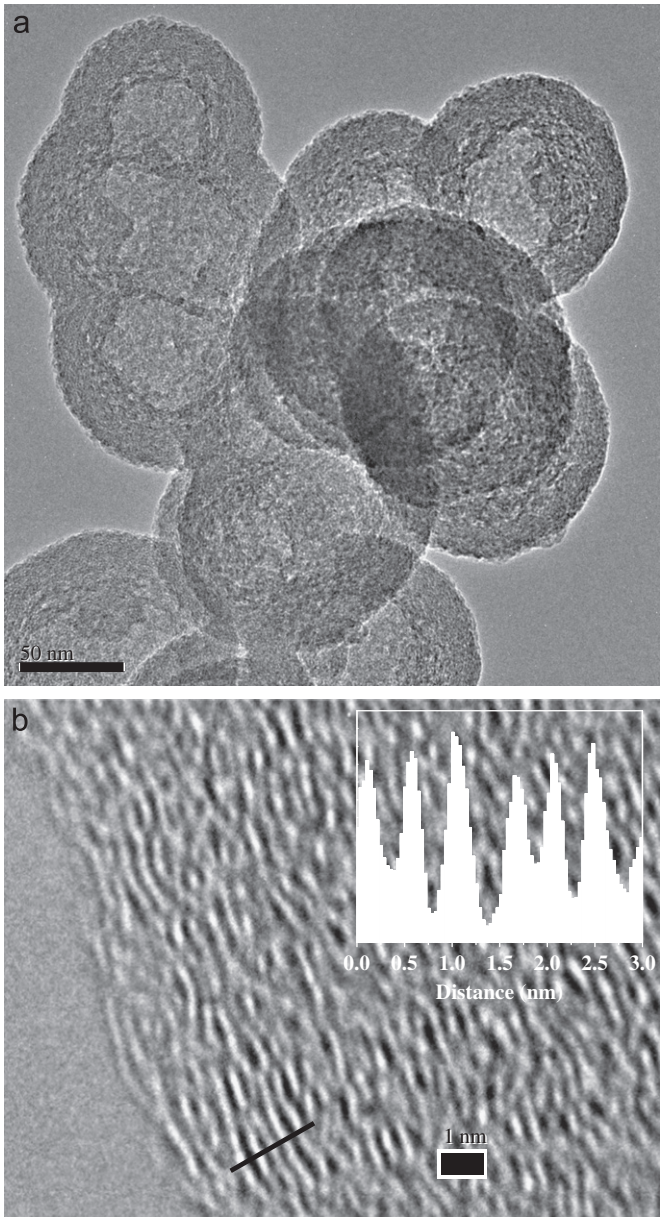

Fig. 7. (a) TEM image of BC_2N prepared by gas phase reaction and (b) HRTEM of the corresponding sample.

[27–29]. Curling occurs in the carbon systems due to the formation of five-member rings but in BN, because five member ring requires B–B and N–N bonds, four member rings may be involved in curling [29]. In the compositions obtained by us curling might happen due to a combined effects of both (see Fig. 2).

The infra-red spectrum of BCN in Fig. 9(a) shows a band around 1400 cm^{-1} due to the in-plane bond stretching. A broad peak centered around 750 cm^{-1} may correspond to the out-of-plane bending mode. The Raman spectrum of BCN in Fig. 10(a) shows bands at 1300 and 1600 cm^{-1}, the latter being similar to the G band of sp^2 carbon systems.

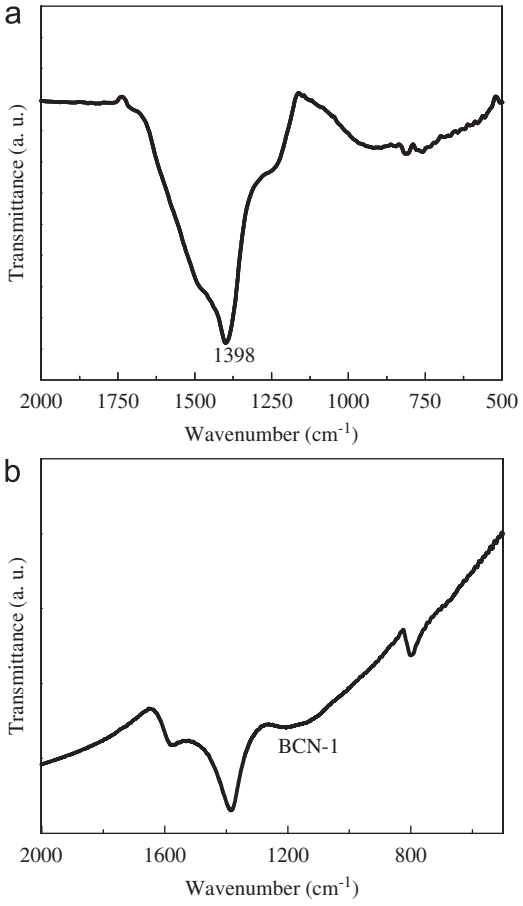

Fig. 9. IR spectra of BCN prepared by (a) gas phase reaction and (b) urea method.

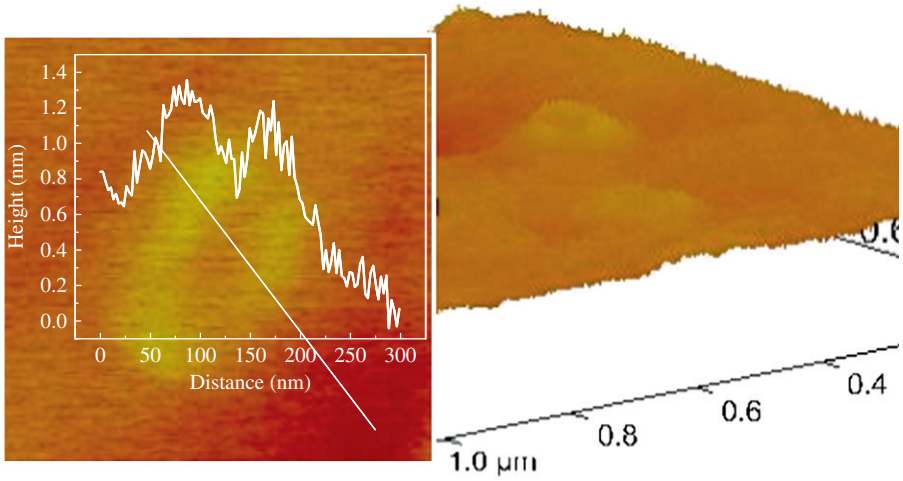

Fig. 8. AFM image of a BCN nano-pan prepared by gas phase reaction along with the height profile.

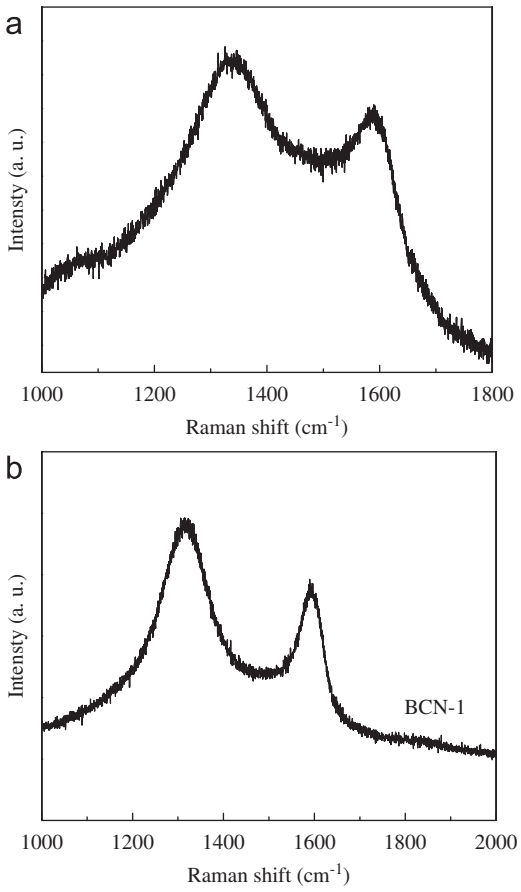

Fig. 10. Raman spectra of BCN prepared by (a) gas phase reaction and (b) urea method.

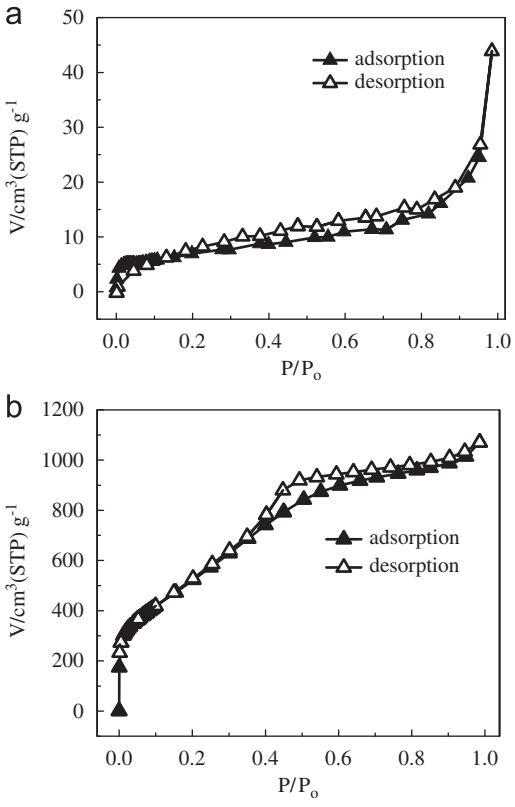

Fig. 11. N_2 adsorption–desorption curves at 77 K and 1 atm for the samples prepared by (a) gas phase synthesis and (b) urea method.

Nitrogen adsorption–desorption curves of BCN are shown in Fig. 11(a). These data show limited nitrogen uptake, with a BET surface area of 25 m^2/g. Thermogravimetric analysis (TGA) of BCN shows it to have a slightly higher thermal stability than graphene or activated charcoal. BCN decomposes fully at ~740 °C in air compared to activated charcoal, which decomposes at 690 °C.

We have prepared compositions of the type BC_xN where x varies between 1 and 2 by the high-temperature reaction of urea and boric acid with high surface area activated charcoal [17]. Some of the samples prepared at 900 °C show compositions close to BCN. These samples show XRD patterns similar to BCN synthesized by the gas phase reaction as can be seen from Fig. 5(b). They also show similar IR and Raman spectra as shown in Figs. 9(b) and 10(b), respectively. TEM images of the samples showed the presence of graphene-like layers them to possess a layered structure. Unlike the BCN samples prepared by gas phase reaction, the BET surface areas of the BCN samples from the urea route are very high, the highest and the lowest values being 1990 and 1500 m^2/g, respectively. In Fig. 11(b), we show the N_2 adsorption and desorption data of the BCN sample possessing the highest surface area (1990 m^2/g) by the urea route.

4. Conclusions

In conclusion, we have been able to synthesize a composition close to BC_xN (x=1.6–1.8) by the gas phase reaction involving BBr_3, ethylene and ammonia. These materials take shape of nanopans. The $B_xC_yN_z$ compositions prepared by this method have low surface areas. In contrast, similar compositions prepared by the urea method, possess high surface areas. All the $B_xC_yN_z$ compositions possess graphene-like layers. First-principles calculations show that the most stable structures of BCN and BC_2N is the one which involves arm-chair type of interface between BN-rich and carbon-rich regions.

References

[1] H.S.S.R. Matte, A. Gomathi, A.K. Manna, D.J. Late, R. Dadtta, S.K. Pati, C.N.R. Rao, Angew. Chem. Int. Ed. 49 (2010) 4059.
[2] A. Nag, K. Raidongia, K.P.S.S. Hembram, R. Datta, U.V. Waghmare, C.N.R. Rao, ACS Nano. 4 (2010) 1539.
[3] S.Y. Kim, J. Park, H.C. Choi, J.P. Ahn, J.Q. Hou, H.S. Kang, J. Am. Chem. Soc. 129 1705 (2007).
[4] L.W. Yin, Y. Bando, D. Golberg, A. Gloter, M.S. Li, X. Yuan, T. Sekiguchi, J. Am. Chem. Soc. 127 (2005) 16354.
[5] M.O. Watanabe, S. Itoh, T. Sasaki, K. Mizushima, Phys. Rev. Lett. 77 (1996) 187.
[6] Y. Chen, J.C. Barnard, R.E. Palmer, M.O. Watanabe, T. Sasaki, Phys. Rev. Lett. 83 (1999) 2406.
[7] W.L. Wang, X.D. Bai, K.H. Liu, Z. Xu, D. Golberg, Y. Bando, E.G. Wang, J. Am. Chem. Soc. 128 (2006) 6530.
[8] R. Ma, D. Golberg, Y. Bando, T. Sasaki, Phil. Trans. R. Soc. Lond. A 362 (2004) 2161.
[9] R. Sen, B.C. Satishkumar, A. Govindaraj, K.R. Harikumar, G. Raina, J.P. Zhang, A.K. Cheetham, C.N.R. Rao, Chem. Phys. Lett. 287 (1998) 671.
[10] O. Stephan, P.M. Ajayan, C. Colliex, P. Redlich, J.M. Lambert, P. Bernier, P. Lefin, Science 266 1683 (1994).
[11] Z. Wengsieh, K. Cherrey, N.G. Chopra, X. Blase, Y. Miyamoto, A. Rubio, M.L. Cohen, S.G. Louie, A. Zettl, A.R. Gronsky, Phys. Rev. B 51 (1995) 11229.
[12] P. Redlich, J. Loeffler, P.M. Ajayan, J. Bill, F. Aldinger, M. Ruhle, Chem. Phys. Lett. 260 (1996) 465.
[13] M. Terrones, N. Grobert, N. Terrones, Carbon 40 1665 (2002).
[14] H.P. Baldus, M. Jansen, Angew. Chem. Int. Ed. 36 (1997) 328.
[15] L.V. Wüllen, M. Jansen, Solid State Nucl. Magn. Resonance 27 (2005) 271.
[16] A. Vinu, M. Terrones, D. Golberg, S. Hishita, K. Ariga, T. Mori, Chem. Mater. 17 (2005) 5887K.
[17] Raidongia, A. Nag, K.P.S.S. Hembram, U.V. Waghmare, R. Datta, C.N.R. Rao, Chem. Eur. J. 16 (2010) 149.
[18] L. Ci, L. Song, C. Jin, D. Jariwala, D. Wu, Y. Li, A. Srivastava, Z.F. Wang, K. Storr, L. Balicas, F. Liu, P.M. Ajayan, Nat. Mater. 9 (2010) 430.

[19] R.B. Kaner, J. Kouvetakis, C.E. Warble, M.L. Sattler, N. Bartlett, Mater. Res. Bull. 22 (1987) 399.
[20] S. Baroni, A. Dal Corso, S. de Gironcoli, P. Gianozzi, 〈http://www.pwscf.org〉.
[21] J.P. Perdew, K. Burke, M. Ernzerhof, Phys. Rev. Lett. 77 (1996) 3865.
[22] D. Vanderbilt, Phys. Rev. B. 41 (1990) 7892.
[23] M. Methfessel, A. Paxton, Phys. Rev. B. 40 (1989) 3616.
[24] L.S. Panchakarla, K.S. Subrahmanyam, S.K. Saha, A. Govindaraj, H.R. Krishnamurthy, U.V. Waghmare, C.N.R. Rao, Adv. Mater. 21 (2009) 4726.
[25] K. Raidongia, K.P.S.S. Hembram, U.V. Waghmare, M. Eswaramoorthy, C.N.R. Rao, Zeit. Anorg. Allg. Chem. 636 (2009) 30.
[26] K. Yamamoto, M. Keunecke, K. Bewilogua, Zs. Czigany, L. Hultman, Surf. Coat. Technol. 142 (2001) 881.
[27] F. Banhart, M. Zwanger, H.J. Muhr, Chem. Phys. Lett. 231 (1994) 98.
[28] O. Stephan, Y. Bando, A. Loiseau, F. Willaime, N. Shramchenko, T. Tamiya, T. Sato, Appl. Phys. A 67 (1998) 107.
[29] F. Xu, Y. Xie, X. Zhang, S. Zhang, X. Liu, X. Tian, Inorg. Chem. 43 (2004) 822.